

Premelting induced smoothening of the ice/vapor interface

Jorge Benet,[‡] Pablo Llombart, Eduardo Sanz and Luis G. MacDowell[†]

*Departamento de Química-Física, Facultad de Ciencias Químicas,
Universidad Complutense de Madrid, 28040 Madrid, Spain**

We perform computer simulations of the quasi-liquid layer of ice formed at the ice/vapor interface close to the ice Ih/liquid/vapor triple point of water. Our study shows that the two distinct surfaces bounding the film behave at small wave-lengths as atomically rough and independent ice/water and water/vapor interfaces. For long wave-lengths, however, the two surfaces couple, large scale parallel fluctuations are inhibited and the ice/vapor interface becomes smooth. Our results could help explaining the complex morphology of ice crystallites.

Nakaya summarized his research on snow flakes in a famous Haiku: "they are letters sent to us from the sky" [1]. Indeed, the habit of ice crystals grown from bulk vapor change from plates, to columns, to plates and yet back to columns as temperature is cooled down below the triple point, with the well known dendritic patterns appearing at sufficiently high super-saturations.[2] Accordingly, the final growth form of a tiny ice crystal conveys detailed information on the atmosphere where it grew.[3]

At a macroscopic level, it is well known that changes in ice crystal habits result from a crossover in the growth rates of the basal and prismatic faces, but exactly what structural transformations occur on the surface to drive this crossover is far from being understood.[1, 2, 4, 5] Kuroda and Lacmann explained the crossover in crystal growth rates as a result of the formation of a thin *quasi-liquid* layer on the ice surface which could set up at different temperatures depending on the crystal facet.[6]

The hypothesis that ice could exhibit a quasi-liquid layer dates back to Faraday, and the formation of such layer on solid surfaces is now well characterized theoretically as a premelting surface phase transition.[7] Experimentally, the advent of modern optical and surface scattering techniques has allowed to gather ample evidence as regards the existence of a premelting liquid film on the surface of ice.[8–14] Unfortunately, the relatively high vapor pressure of ice makes it very difficult to achieve sizeable equilibrium crystals,[2] while the presence of impurities has a very large impact on surface structure.[12, 15] Accordingly, many other relevant properties, such as the premelting temperature, the thickness of the quasi-liquid layer or the presence of surface melting remain a matter of debate.[8]

One particularly important structural property with large impact on crystal growth rates is the surface roughness.[6, 16, 17] Contrary to smooth or singular facets, which have a limited number of defects and serve as basis for most crystal growth models, rough surfaces present diverging height fluctuations which do not differ macroscopically to those found in a fluid interface. As a result, rough crystal planes with correlation lengths that are larger than the crystallite disappear and become round.[18–20] More importantly, as far as crystal

habits and growth forms are concerned, the roughening of a surface has dramatic consequences on the dynamics, as it signals a crossover from a two dimension nucleated growth, to a faster Knudsen mechanism that is linear in the saturation.[6, 17] Unfortunately, this phenomenology has been established only for rather simple interfaces,[17] and the role of a premelting film in the surface roughness is largely unknown.

Here we perform computer simulations of a premelting layer on the primary prismatic facet of the ice/vapor interface. Our study reveals that the structure and fluctuations of the surfaces bounding the quasi-liquid layer at small length-scales are very much like those of atomically rough and independent ice/water and water/vapor interfaces. However, the finite equilibrium thickness of the premelting layer below the triple point drives the long-wavelength structure of the interface from rough to smooth. Our results clarify why the facets of ice crystals remain recognizable up to the triple point, and suggest the formation of a premelting layer could slow down growth kinetics, as required to explain ice crystal growth habits in the atmosphere.[6]

Our study is performed with the TIP4P/2005 model of water, [21] which has been shown to reproduce with remarkable accuracy a large number of bulk and surface properties of (liquid) water and ice.[22] A slab of equilibrated bulk ice with several thousand molecules is placed in contact with vacuum inside a large orthorhombic simulation box, such that an interface of surface area $A = L_x L_y$ is exposed parallel to the xy plane. Surfaces thus prepared exhibit a very large heterogeneity of vacancy energies, with a strong dependence on the proton ordering arrangements.[23] For this reason we prepare our initial samples using a special purpose Monte Carlo algorithm that suitably samples the hydrogen bond network.[24–26] Averages are then collected using Molecular Dynamics with the Gromacs package for about half a microsecond,[27–35] well above the expected relaxation time for the ice/water interface.[36] Performing the simulations along the sublimation line at a temperature $\Delta T = T - T_t$ just 2 K below the triple point temperature, T_t , [37] the first few ice layers melt and form a premelting quasi-liquid layer (Fig.1), as noticed earlier.[38–41] The nature

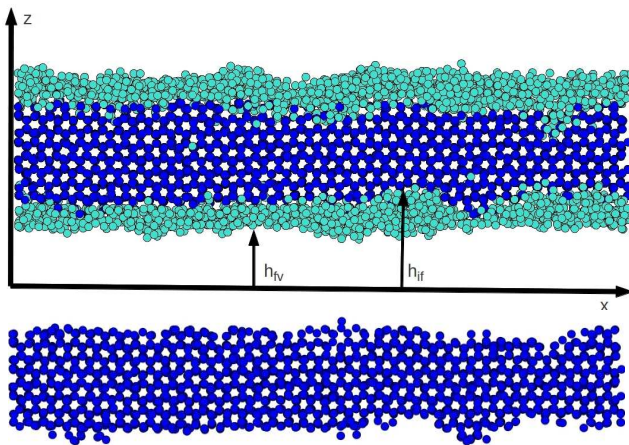


FIG. 1. Snapshot of the ice/vapor interface during the course of our simulations. Top: A quasi-liquid layer of disordered molecules is clearly seen on top of bulk ice. The order parameter allows us to distinguish between an ice/film and a film/vapor surface. Bottom: Same figure with liquid-like atoms removed.

and size of this layer may be quantified using the \bar{q}_6 order parameter,[42] which has been optimized to discriminate ice like and water like molecules from a study of molecular correlations up to second nearest neighbors.[43] To get rid of vapor molecules, we identify the premelting layer as the largest cluster of water molecules, and find an average thickness of $\ell = 0.9$ nm, in reasonable agreement with experimental observations,[12, 14] and recent simulations.[38–40] Here, we attempt to characterize the quasi-liquid film in terms of two fluctuating ice/film (if), and film/vapor (fv) surfaces, which we locate by locally averaging the heights of the outermost solid and liquid molecules of the layer, respectively (Fig.1). Comparing our results for the ice/vapor interface with our previous study of the ice/water interface will prove insightful.[44] Since we aim at studying large wavelength fluctuations, we prepare the exposed faces with an elongated geometry, with box side $L_x \gg L_y$. This allows us to identify ice/film, $h_{if}(x)$ and film/vapor $h_{fv}(x)$ surface profiles along the largest axis, x . These film profiles are then Fourier transformed to yield the spectrum of surface fluctuations.[27]

For the purpose of studying the fluctuations of the quasi-liquid layer, it is convenient to define the quantity $\Gamma_{\alpha\beta}(q_x)$, in terms of the thermal averages of Fourier amplitudes $h_{\alpha\beta}$, as:

$$\Gamma_{\alpha\beta}(q_x) = \frac{k_B T}{A \langle h_{\alpha\beta}(q_x) h_{\alpha\beta}^*(q_x) \rangle q_x^2} \quad (1)$$

where k_B is Boltzmann's constant, $q_x = 2\pi n/L_x$, and n is a positive integer. According to Capillary Wave Theory,[45] for a rough interface between bulk phases

α and β , the function $\Gamma_{\alpha\beta}(q_x)$ may be identified with a wave-vector dependent stiffness, $\tilde{\gamma}_{\alpha\beta}(q_x)$ whose $q_x \rightarrow 0$ limit is the macroscopic stiffness of the interface,[46–48] corresponding exactly to the surface tension for fluid/fluid interfaces.[49, 50] In the forthcoming exposition we concentrate on the primary prismatic plane (pI) at $\Delta T = -2$ K and study the fluctuations propagated along the basal [Basal] and secondary prismatic [pII] directions.

The results, $\Gamma_{if}(q_x)$ and $\Gamma_{fv}(q_x)$ obtained for the ice/film and film/vapor surface fluctuations of the premelting layer on the primary prismatic plane, either along [Basal] or [pII] orientations agree very nicely with those obtained for the corresponding ice/water, $\Gamma_{iw}(q_x)$, and water/vapor, $\Gamma_{wv}(q_x)$, interfaces down to $q_x^* 1.5 \text{ nm}^{-1}$ (Fig.2.a-b). This implies that for a quasi-liquid layer hardly one nanometer thick, the ice/film and film/vapor surfaces at this length-scales fluctuate independently, with fluctuations that can hardly be distinguished from those found at the rough interfaces of bulk water. Interestingly, at $q_x \approx q_x^*$, $\Gamma_{iw}(q_x)$ and $\Gamma_{wv}(q_x)$ are already close to their $q_x \rightarrow 0$ limit, and are therefore close to the corresponding macroscopic stiffness coefficients.

The striking resemblance between the surface fluctuations of the quasi-liquid layer and bulk water for $q_x > q_x^*$ can be understood in terms of the density profiles shown in Fig.3 for the primary prismatic plane (with similar results found for the basal and secondary prismatic planes, c.f. Ref.27). Indeed, the density profile of solid-like molecules from the ice/vapor interface (full-red) almost matches that observed at the ice/water interface (dashed-indigo). Similarly, the profile of liquid-like molecules of the quasi-liquid layer at the ice/vapor interface (full-blue) is very similar to that at the ice/water interface (dashed-green) until the very end of the premelting film, where it obviously drops to the values expected for the bulk vapor density.

Below q_x^* , the fluctuating surfaces start noticing the finite thickness of the quasi-liquid layer, as implied by the departure of $\Gamma_{if}(q_x)$ and $\Gamma_{fv}(q_x)$ from the ice/water and water/vapor behavior. For the fluctuations in the (pI)[pII] direction, a sharp rise of $\Gamma(q_x)$ for both the ice/film and film/vapor surfaces suggest a divergence as $q_x \rightarrow 0$, and indicate the onset of a completely different regime, with finite correlations at infinite wavelengths and an effective infinite stiffness coefficient (Fig.2.a). For the fluctuations in the (pI)[Basal] direction, on the contrary, $\Gamma(q_x)$ rises above the values expected for the ice/water and water/vapor interfaces, but seems to attain a finite asymptotic limit for $q_x \rightarrow 0$ (Fig.2.b). These conflicting results for the (pI) interface at $\Delta T = -2$ K indicate the proximity of a *roughening transition*, where the interface depins from the underlying bulk solid. Roughening is a Kosterlitz-Thoules transition of infinite order.[20] Not unexpectedly, the error bars observed for $\Gamma(q_x)$ are extremely large, and sub-averages may be col-

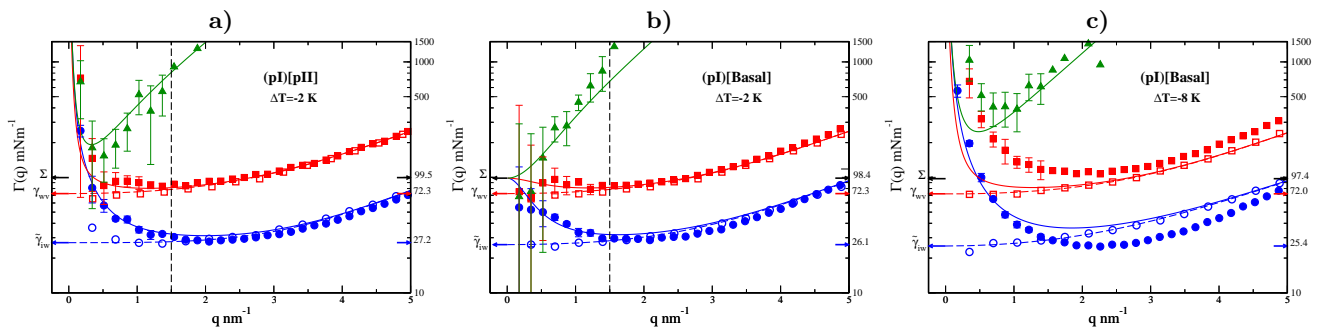


FIG. 2. Fluctuations of the premelting film on the primary prismatic plane. The plot displays effective wave-vector dependent stiffness, $\Gamma(q_x)$ in log scale for (pI)[pII] at $\Delta T = -2$ K (a); and (pI)[Basal] at $\Delta T = -2$ K (b) and $\Delta T = -8$ K (c). Results for the quasi-liquid layer are shown with filled symbols, with $\Gamma_{if}(q_x)$ for the ice/film (blue circles) and $\Gamma_{fv}(q_x)$ for the film/vapor surfaces (red squares). The open symbols are results for the ice/water (blue circles) and water/vapor (red squares) interfaces, which are fitted to $\Gamma(q_x) = \gamma + \kappa q_x^2 + \epsilon q_x^4$ (dashed lines) for the purpose of extrapolation (c.f. Ref.44 and 27). The colored arrows indicate extrapolation to $q_x = 0$, which provides the ice/water stiffness $\tilde{\gamma}_{iw}$ and the water/vapor surface tension, γ_{wv} , respectively. The black arrow points to $\Sigma = \tilde{\gamma}_{iw} + \gamma_{wv}$, where the effective stiffness of the quasi-liquid film would converge were the interface rough. The dashed vertical line indicates approximately the regime of q_x where the quasi-liquid surfaces cease to behave independently. The green triangles indicate results for the coupled fluctuations of the ice/film and film/vapor surfaces, $\Gamma_{iv}(q_x)$. Full lines are results from a fit to the model of Eq. (4).

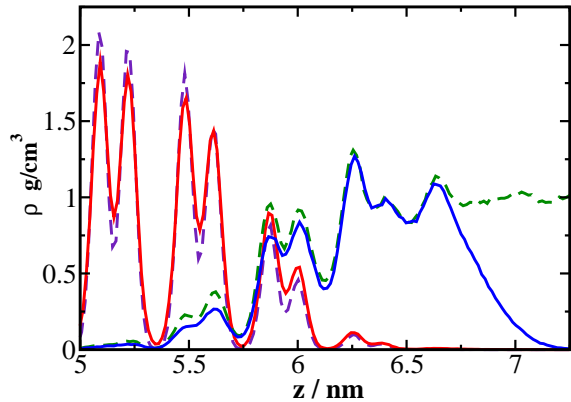


FIG. 3. Structure of the ice/vapor (full lines) and ice/liquid (dashed lines) interfaces of the primary prismatic plane along the perpendicular direction. The density of solid-like molecules is shown in full-red for the solid/vapor interface and in dashed-indigo for the solid/liquid interface. The density of liquid-like molecules is shown in full-blue for the solid/vapor interface and in dashed-green for the solid/liquid interface.

lected which appear consistent with either a rough or a smooth interface. By simulating the same interfaces just 6 K below, we find that $\Gamma(q_x)$ also becomes divergent for the (pI)[Basal] direction, confirming the smoothing of the interface just a few Kelvin below the triple point (as expected the divergence remains for (pI)[pII] direction, c.f. Ref.27). This result is consistent with the rounding of edges between prismatic facets observed in simulations of ice micro-crytallites.[40]

The observation of a roughening transition at about $\Delta T = -2$ K is somewhat puzzling. Given the similarity between the structure of the quasi-liquid layer and bulk water at short length scales, why are the long wave-

length fluctuations so different? Here we show how the finite thickness of the premelting film can change completely the low wave-vector response of the ice/film and film/vapor surfaces even under the assumption that the corresponding stiffness coefficients are exactly those of rough ice/water and water/vapor interfaces, respectively.

To see this, we consider the sine-Gordon model of the solid/liquid interface,[20, 45] and assume that the free energy of the ice/film layer is given solely in terms of parameters akin to the ice/water interface:

$$H_{if} = \int dx \left(\frac{1}{2} \tilde{\gamma}_{iw} (\nabla h_{if})^2 - u \cos(k_z h_{if}) \right) \quad (2)$$

where $\tilde{\gamma}_{iw}$ is the interface stiffness, $k_z = \frac{2\pi}{b}$ and b is the inter-plane spacing. In this model, the square gradient term penalizes the departure of the ice/film layer from planarity, while the cosine term favors by an amount u those configurations where $h_{if}(\mathbf{x})$ is a multiple of the lattice spacing. For the film/vapor surface, we consider that the free energy is described by capillary wave theory, with departures from planarity penalized by the water/vapor surface tension, γ_{wv} : [51]

$$H_{fv} = \int dx \left(\frac{1}{2} \gamma_{wv} (\nabla h_{fv})^2 + g(\Delta h) \right) \quad (3)$$

For an inert substrate, $g(\Delta h)$ is the interface potential, which dictates the free energy of a planar premelting film of height Δh . [52] In our model, it plays the crucial role of coupling the film/vapor fluctuations to the ice/film surface, since $\Delta h = h_{fv} - h_{if}$.

To solve for this coupled Capillary Wave + sine-Gordon model approximately, we extend a variational theory for the sine-Gordon model due to Safran.[45] The

solution yields the Fourier modes of surface fluctuations, as follows:[27]

$$\begin{aligned} \langle |h_{\text{if}}^2(q_x)| \rangle &= \frac{k_B T}{A} \frac{g'' + \gamma_{wv} q_x^2}{w g'' + (g'' \Sigma + w \gamma_{wv}) q_x^2 + \gamma^2 q_x^4} \\ \langle |h_{\text{fv}}^2(q_x)| \rangle &= \frac{k_B T}{A} \frac{w + g'' + \tilde{\gamma}_{iw} q_x^2}{w g'' + (g'' \Sigma + w \gamma_{wv}) q_x^2 + \gamma^2 q_x^4} \\ \langle h_{\text{if}}(q_x) h_{\text{fv}}^*(q_x) \rangle &= \frac{k_B T}{A} \frac{g''}{w g'' + (g'' \Sigma + w \gamma_{wv}) q_x^2 + \gamma^2 q_x^4} \end{aligned} \quad (4)$$

where g'' is the second derivative of the interface potential with respect to the layer thickness, $\Sigma = \tilde{\gamma}_{iw} + \gamma_{wv}$, $\gamma^2 = \tilde{\gamma}_{iw} \gamma_{wv}$, while w is a roughness parameter that needs to be solved self-consistently:

$$w = u k_z^2 e^{-\frac{1}{2} k_z^2 \sum_{\mathbf{q}} \langle |h_{\text{if}}^2(\mathbf{q})| \rangle} \quad (5)$$

Notice that the sum over wave-vectors confers to w a dependence on the surface geometry.[27]

The above result nicely rationalizes our observations. At large wave-vectors, $q \rightarrow \infty$, the system is *atomically rough*, i.e. $\Gamma_{\text{if}}(q_x) \rightarrow \tilde{\gamma}_{iw}$ and $\Gamma_{\text{fv}}(q_x) \rightarrow \gamma_{wv}$, whence the ice/film and film/vapor surfaces behave as rough ice/water and water/vapor interfaces as observed in Fig.2 (a and b).

Furthermore, the fluctuations are then fully independent. This can be seen by considering the cross correlations, $\langle h_{\text{if}}(q_x) h_{\text{fv}}^*(q_x) \rangle$, which in this limit fall to zero. Defining the related function $\Gamma_{\text{iv}}(q_x) = k_B T / A \langle h_{\text{if}}(q_x) h_{\text{fv}}^*(q_x) \rangle q_x^2$, consistent with Eq. (1), we find indeed that our simulation results for $\Gamma_{\text{iv}}(q_x)$ diverge at large q (see Fig.2). This regime of large wave-vectors is consistent with observations by Limmer and Chandler, who measured a stiffness coefficient from the ice/film fluctuations in reasonable agreement with results for the ice/liquid interface in their simulations.[41] In the limit of small wave-vectors, $q_x \rightarrow 0$, however, we get qualitatively different behaviors depending on the roughness parameter (c.f. Fig.6 Ref.27). On the one hand, if $w = 0$, the fluctuations diverge, and both surfaces behave as rough interfaces with stiffness Σ , (i.e. $\Gamma_{\text{if}}(0) = \Gamma_{\text{fv}}(0) = \Gamma_{\text{iv}}(0) = \Sigma$). On the other hand, if $w \neq 0$, the fluctuations remain finite as $q_x \rightarrow 0$, whence $\Gamma_{\alpha\beta}(q_x)$ diverges as q_x^{-2} , indicating a smooth interface. Despite the atomic roughness at small length-scales, the smoothening of the surface has dramatic consequences, since both the crystal shape and crystal growth rate is dictated by $\Gamma_{\text{if}}(\mathbf{q} \rightarrow 0)$. [17–19, 45]

In our simulations at $\Delta T = -2$ K, we observe, for the (pI)[Basal] direction, a behavior consistent with $w = 0$, corresponding to a rough interface (Fig.2.b). For (pI)[pII] direction, on the contrary, we clearly observe for the smallest wave-vector accessible that $\Gamma_{\text{fv}}(q_x)$ has largely exceeded Σ , while $\Gamma_{\text{iv}}(q_x)$ attains a minimum well above

Σ , and then exhibits a strong divergence, as predicted by our model for a smooth interface (Fig.2.a). This ‘roughness anisotropy’ is consistent with Eq. (5), which indicates that the roughening temperature for our (pI)[pII] system could be higher than that of the (pI)[Basal] system by a factor ≈ 1.01 given by the ratio of the ice/vapor stiffness coefficients (Σ). [27]

The qualitative statements that result from our model may be made quantitative and extended to large wave-vectors provided we replace $\tilde{\gamma}_{iw}$ and γ_{wv} in Eq. (4) by the phenomenological wavevector dependent coefficients $\tilde{\gamma}_{iw}(q_x)$, and $\gamma_{wv}(q_x)$ obtained from the simulations of the ice/water and water/vapor interfaces. A least square fit to the Fourier amplitudes of (pI) at $\Delta T = -2$ K, yields $g'' \approx 8 \cdot 10^{15}$ J/m⁴ for both directions, while the roughness parameter is $w = 0$ for the (pI)[Basal] direction and $w = 3.3 \cdot 10^{15}$ J/m⁴ for the (pI)[pII] direction, indicative of the proximity of a roughening transition. At $\Delta T = -8$ K, the fit for both directions is consistent with $g'' \approx 12 \cdot 10^{15}$ J/m⁴ and $w \approx 8 \cdot 10^{15}$ J/m⁴, corresponding to a smooth interface.

But how can the surface of the ice/film interface become smooth for small wave-vectors while the small wavelength structure remains essentially equal to that of a film of infinite depth? This question can be answered by solving for the self-consistent condition, Eq. (5), with the help of Eq. (4). The result gives w as the root of a transcendental equation.[27] For a film of infinite height, with $g'' = 0$, we obtain:

$$w \propto \left(1 + \frac{\tilde{\gamma}_{iw}}{w} q_{max}^2 \right)^{-\tau_{iw}} \quad (6)$$

where q_{max} is an upper wave-vector cutoff for the fluctuations. The above result corresponds to the approximate solution of the sine-Gordon model due to Safran.[45] The resulting transcendental equation depends essentially on one parameter $\tau_{iw} = \frac{k_B T k_z^2}{8\pi \tilde{\gamma}_{iw}}$. For $\tau_{iw} > 1$, the root is $w = 0$, and the surface is rough, while for $\tau_{iw} < 1$, the root is finite, and the surface is smooth. For films of finite depth, $g'' > 0$, and the situation changes. The roots are still governed by an equation similar to the above result:

$$w \propto \left(1 + \frac{\Sigma}{w} q_{max}^2 \right)^{-\mu_{\text{if}}} \quad (7)$$

but now the exponent is $\mu_{\text{if}} = \frac{\tilde{\gamma}_{iw}}{\Sigma} \cdot \tau_{iw}$, which is always smaller than τ_{iw} . [27] Whence, for a rough ice/water surface with τ_{iw} close but greater than unity, μ_{if} will be well smaller than unity, and the corresponding ice/film surface will become smooth, even though the ice/water surface is rough. Surprisingly, the exponent dictating the transition does not depend on the thickness of the layer, as long as g'' is finite. Only the precise value of w is dictated by the premelting thickness.[27]

Our theoretical approach explains our simulation results and is consistent with experimental observations.

The roughening transition of the prismatic plane has been measured for ice crystals in water[53] and vapor[9, 54]. It is found that from $\Delta T \approx -16$ K up to the triple point, the ice/water interface is rough, while, due to the limited width of the quasi-liquid layer, the ice/film surface remains smooth up to about $\Delta T \approx -4$ to -2 K, as suggested in our simulations. In fact, in the atmosphere ice crystals exhibit faceted prismatic faces up to 0 C, even at very low saturation.[2] Since smooth surfaces have a slow activated dynamics, our results suggest it is the formation of the quasi-liquid layer what could actually slow down the crystal growth rates and provide a mechanism for the change of crystal habits, as hypothesized by Kuroda and Lacmann [6].

In summary, we have shown that close to the triple point a quasi-liquid layer of premelting ice on the primary prismatic face behaves as two independent ice/water and water/vapor surfaces at small wavelengths, but becomes smooth at long wavelengths. Our results may help rationalize the role of the premelting layer in the morphology of ice crystals.

E. Sanz and J. Benet acknowledge financial support from the EU grant 322326-COSAAC-FP7-PEOPLE-2012-CIG and from a Spanish grant Ramon y Cajal. L.G. MacDowell acknowledges financial support from project MAT-2014-59678-R (Ministerio de Economía y Competitividad).

J.B. and P.L. contributed equally to this work.

* †lgmac@quim.ucm.es; ‡Department of Physics, University of Durham, South Road, Durham DH1 3LE, United Kingdom

[1] I. Sunagawa, ed., *Morphology of Crystals* (Terra Scientific Publishing Company, Tokyo, 1987).

[2] K. G. Libbrecht, Rep. Prog. Phys. **68**, 855 (2005).

[3] H. R. Pruppacher and J. D. Klett, *Microphysics of Clouds and Precipitation* (Springer, Heidelberg, 2010).

[4] X. Y. Liu, E. S. Boek, W. J. Briels, and P. Bennema, Nature **374**, 342 (1995).

[5] Y. Furukawa and J. Wettlaufer, Phys. Today **60**, 70 (2007).

[6] T. Kuroda and R. Lacmann, J. Cryst. Growth **56**, 189 (1982).

[7] R. Lipowsky, Phys. Rev. Lett. **49**, 1575 (1982).

[8] J. G. Dash, A. W. Rempel, and J. S. Wettlaufer, Rev. Mod. Phys. **78**, 695 (2006).

[9] M. Elbaum, Phys. Rev. Lett. **67**, 2982 (1991).

[10] A. Lied, H. Dosch, and J. H. Bilgram, Phys. Rev. Lett. **72**, 3554 (1994).

[11] H. Dosch, A. Lied, and J. H. Bilgram, Surf. Sci. **327**, 145 (1995).

[12] H. Bluhm, D. F. Ogletree, C. S. Fadley, Z. Hussain, and M. Salmeron, J. Phys.: Condens. Matter **14**, L227 (2002).

[13] G. Sazaki, S. Zepeda, S. Nakatsubo, M. Yokomine, and Y. Furukawa, Proc. Nat. Acad. Sci. **109**, 1052 (2012), <http://www.pnas.org/content/109/4/1052.full.pdf>.

[14] K.-i. Murata, H. Asakawa, K. Nagashima, Y. Furukawa, and G. Sazaki, Phys. Rev. Lett. **115**, 256103 (2015).

[15] J. Wettlaufer, Phys. Rev. Lett. **82**, 2516 (1999).

[16] W. K. Burton, N. Cabrera, and F. C. Frank, Phyl. Trans. R. Soc. Lond. A **243**, 299 (1951).

[17] J. D. Weeks and G. H. Gilmer, Adv. Chem. Phys. **40**, 157 (1979).

[18] C. Jayaprakash, W. F. Saam, and S. Teitel, Phys. Rev. Lett. **50**, 2017 (1983).

[19] C. Rottman and M. Wortis, Phys. Rev. B **29**, 328 (1984).

[20] P. M. Chaikin and T. C. Lubensky, *Principles of Condensed Matter Physics* (Cambridge University Press, Cambridge, 1995).

[21] J. L. F. Abascal and C. Vega, J. Chem. Phys. **123**, 234505 (2005).

[22] C. Vega and J. L. F. Abascal, Phys. Chem. Chem. Phys. **13**, 19663 (2011).

[23] M. Watkins, D. Pand, E. G. Wang, A. Michaelides, J. VandeVondele, and B. Slater, Nature Materials **10**, 794 (2011).

[24] V. Buch, P. Sandler, and J. Sadlej, J. Phys. Chem. B **102**, 8641 (1998).

[25] S. W. Rick and A. D. J. Haymet, J. Chem. Phys. **118**, 9291 (2003).

[26] L. G. MacDowell and C. Vega, J. Phys. Chem. B **114**, 6089 (2010).

[27] “See supplemental material for the model and simulation details and theory, which includes Refs.[28-35],”.

[28] G. Bussi, D. Donadio, and M. Parrinello, J. Chem. Phys. **126**, 014101 (2007).

[29] K. Rommelse and M. den Nijs, Phys. Rev. Lett. **59**, 2578 (1987).

[30] N. Goldenfeld, *Lectures on Phase Transitions and the Renormalization Group* (Perseus Books, Reading, Massachusetts, 1992).

[31] L. G. MacDowell, [cond-mat.soft] , ArXiv:1512.04777 (2015).

[32] N. Akutsu, Y. Akutsu, and T. Yamamoto, Phys. Rev. B **64**, 085415 (2001).

[33] D. S. Fisher and J. D. Weeks, Phys. Rev. Lett. **50**, 1077 (1983).

[34] N. Akutsu and T. Yamamoto, in *Handbook of Crystal Growth (Second Edition)*, edited by T. Nishinaga (Elsevier, Boston, 2015) second edition ed., pp. 265–313.

[35] J. Benet, L. G. MacDowell, and E. Sanz, J. Chem. Phys. **142**, 134706 (2015), <http://dx.doi.org/10.1063/1.4916398>.

[36] J. Benet, L. G. MacDowell, and E. Sanz, J. Chem. Phys. **141**, 034701 (2014).

[37] D. Rozmanov and P. G. Kusalik, Phys. Chem. Chem. Phys. **13**, 15501 (2011).

[38] M. M. Conde, C. Vega, and A. Patrykiewicz, J. Chem. Phys. **129**, 014702 (2008).

[39] C. L. Bishop, D. Pan, L. M. Liu, G. A. Tribello, A. Michaelides, E. G. Wang, and B. Slater, Faraday Discuss. **141**, 277 (2009).

[40] D. Pan, L.-M. Liu, B. Slater, A. Michaelides, and E. Wang, ACS nano **5**, 4562 (2011).

[41] D. T. Limmer and D. Chandler, J. Chem. Phys. **141**, 18C505 (2014).

[42] W. Lechner and C. Dellago, J. Chem. Phys. **129**, 114707 (2008).

[43] E. Sanz, C. Vega, J. R. Espinosa, R. Caballero-Bernal, J. L. F. Abascal, and C. Valeriani, J.

- Am. Chem. Soc. **135**, 15008 (2013), PMID: 24010583, <http://dx.doi.org/10.1021/ja4028814>.
- [44] J. Benet, L. G. MacDowell, and E. Sanz, Phys. Chem. Chem. Phys. **16**, 22159 (2014).
- [45] S. A. Safran, *Statistical Thermodynamics of Surfaces, Interfaces and Membranes*, 1st ed. (Addison-Wesley, Reading, 1994).
- [46] J. J. Hoyt, M. Asta, and A. Karma, Phys. Rev. Lett. **86**, 5530 (2001).
- [47] R. L. Davidchack, J. R. Morris, and B. B. Laird, J. Chem. Phys. **125**, 094710 (2006).
- [48] A. Härtel, M. Oettel, R. E. Rozas, S. U. Egelhaaf, J. Horbach, and H. Löwen, Phys. Rev. Lett. **108**, 226101 (2012).
- [49] M. Müller and M. Schick, J. Chem. Phys. **105**, 8282 (1996).
- [50] E. Chacon and P. Tarazona, J. Phys.: Condens. Matter **17**, S3493 (2005).
- [51] D. Nelson, T. Piran, and S. Weinberg, *Statistical Mechanics of Membranes and Surfaces* (World Scientific, Singapore, 2004).
- [52] S. Dietrich, in *Phase Transitions and Critical Phenomena*, Vol. 12, edited by C. Domb and J. L. Lebowitz (Academic, New York, 1988) pp. 1–89.
- [53] M. Maruyama, J. Cryst. Growth **275**, 598 (2005).
- [54] H. Asakawa, G. Sasaki, K. Nagashima, S. Nakatsubo, and Y. Furukawa, Crystal Growth & Design **15**, 3339 (2015), <http://dx.doi.org/10.1021/acs.cgd.5b00438>.

Premelting induced smoothening of the ice/vapor interface

Supplementary material

Jorge Benet, Pablo Llombart, Eduardo Sanz and Luis G. MacDowell

¹*Dep. Química Física, Fac. Química, Universidad Complutense de Madrid, 28040, Spain*

Abstract

This file contains supplementary information on simulations details, additional results for (pI)[pII], (Basal)[pII] and (pII)[Basal] systems and the solution for the coupled Capillary Wave + sine-Gordon model described in the paper.

I. METHODS AND SIMULATION

A. Simulations

Our study is performed with the TIP4P/2005 model of water [1]. A slab of bulk ice is first prepared from scratch using the algorithm of Buch et al.[2] to sample a hydrogen bond network consistent with the ice rules. This initial configuration is then equilibrated with a Monte Carlo simulation that samples over closed hydrogen bond loops using a cluster algorithm by Rick and Haymet.[3, 4] It then undergoes an isotropic NpT simulation in order to obtain the equilibrium lattice parameters at coexistence. The equilibrated ice sample is placed in contact with vacuum inside a large orthorhombic simulation box, such that an interface of surface area $A = L_x L_y$ is exposed parallel to the xy plane. For production runs, we performed NVT Molecular Dynamics simulations with the Gromacs package at temperatures $\Delta T = T - T_t$ of -2 and -8 K, with $T_t = 250$ K the estimated triple point temperature of the model.[5] We use the Bussi-Donadio-Parrinello thermostat.[6] Lennard-Jones interactions are truncated at $R_c = 0.85$ nm, and electrostatic interactions are evaluated using Ewald summations.

The surface waves on a crystal depend on the crystal plane that is exposed, as well as on the direction of propagation. We use the conventional terminology $(\mathbf{u})[\mathbf{n}]$ to designate such fluctuations,[7, 8] where \mathbf{u} is a vector perpendicular to the exposed plane, while \mathbf{n} is a vector perpendicular to \mathbf{u} and the direction of propagation. The vectors \mathbf{u} and \mathbf{n} are designated by the Miller-Bravais indices $\{h,k,l,i\}$ of the hexagonal symmetry group

corresponding to ordinary ice (Ih). For the sake of brevity, we designate sets of equivalent indices corresponding to a given plane or direction as ‘Basal’, for $\{0001\}$, ‘pI’ for $\{10\bar{1}0\}$ and ‘pII’ for $\{2\bar{1}\bar{1}0\}$.

In order to study fluctuations with the largest possible wave-length we prepare the exposed faces with an elongated geometry, with box side $L_x > L_y$ (see Table I for a description of system size and simulation conditions). This allows us to identify ice/film, $h_{if}(x)$ and film/vapor $h_{fv}(x)$ surface profiles along the largest axis, x (see Fig.1 of paper). Accordingly, for fluctuations designated as (hkli)[h’k’l’i’], the plane (hkli) of the interface is perpendicular to the z axis, while the direction [h’k’l’i’] is parallel to the y axis. For ice/vapor systems, we considered a very large lateral size $L_x \approx 36$ nm. On the other hand ice/water interfaces were studied using $L_x \approx 18$ nm.

We choose the crystal orientation such that the primary prismatic plane is exposed (pI). Configurations were prepared with the long direction along either the basal [Basal] or secondary prismatic orientations [pII]. This allows us to measure long wavelength fluctuations, which are denoted as (pI)[Basal] and (pI)[pII], for fluctuations on the (pI) plane along the [Basal] and [pII] directions, respectively. Less detailed results for (Basal)[pII] and (pII)[Basal] geometries with $L_x \approx 18$ nm are also reported in this document (see below).

To simulate ice/water interfaces, we use the configurations prepared for the ice/vapor interface. We then equilibrate a slab of liquid water with equal lateral dimensions than the solid. Both phases are brought together, and molecules of the liquid phase less than one molecular diameter apart are removed. The compound system is then equilibrated in an Np_zT simulation with the barostat along the perpendicular direction to the interface only.[8, 9] For the liquid-vapor interface, it suffices to equilibrate a liquid slab under periodic boundary conditions. The slab is then placed in vacuum and a liquid-vapor interface equilibrates gradually.

B. Location of the interface

Liquid like and solid like molecules are distinguished using the \bar{q}_6 order parameter by Lechner and Dellago [10], which has been optimized to discriminate ice like and water like molecules from a study of molecular correlations up to second nearest neighbors. For the TIP4/2005 model in the range of temperatures studied we chose a threshold value of

$\bar{q}_6 = 0.347$ to discriminate between liquid like and solid like molecules.

To define the film/vapor surface, we define a grid on the xy plane. For each bin on the grid, the position of the interface is determined as an average of the 4 outermost liquid-like molecules contained within a distance $x = 1/2 \cdot \Delta_x$ and $y = 1/2 \cdot \Delta_y$, with $\Delta_x = 0.91$ nm and $\Delta_y = 1/2 \cdot L_y$. A similar procedure is used to evaluate the ice/film surface, with the position of the surface determined from the outermost solid-like molecules. The corresponding surfaces are averaged along the y direction to obtain $h_{\text{if}}(x)$ and $h_{\text{fv}}(x)$. These film profiles are then Fourier transformed to yield the spectrum of surface fluctuations.

The spectrum of the ice/film fluctuations is compared in Fig.2 of the paper with corresponding fluctuations for the ice/liquid interface at the same temperature. For $\Delta T = -2$ K, we employed results obtained previously by ourselves.[9] For $\Delta T = -8$ K, we performed new simulations (see Table I). Having equilibrated the ice/water interface as explained above, the spectrum of fluctuations is calculated exactly as described for the ice/film surface. The solid and liquid bulk phases that were merged to prepare the interface were previously equilibrated at the coexistence pressure of $p = 882$ bar. Similarly, the spectrum for the water/vapor interface is calculated as for the film/vapor interface.

During the course of the simulations, the center of the solid slab fluctuates and blurs the density profile. To avoid this, we collect density profiles for short periods of 37.5 ns. This also helps eliminate capillary wave roughening. Further details of the procedure may be found in Ref.[8, 9].

C. Summary of results for the (pI) plane.

Here we collect all results of $\Gamma(q)$ for the (pI) plane. At $\Delta T = -2$ K, (pI)[Basal] appears rough, and (pI)[pII] appears smooth. At $\Delta T = -8$ K, both sets of fluctuations are consistent with a smooth interface, as can be seen from the divergence of $\Gamma(q)$ in the limit $q \rightarrow 0$ (Fig.1). For $\Delta T = -8$ K, however, the coexistence pressure of the ice/water interface is now about 900 MPa, and the short wave-length fluctuations of the ice/vapor interface differ considerably from the ice/liquid and liquid/vapor results. Note that the presence of atomic roughness at a small lengthscale within a smooth surface is consistent with a pre-roughening scenario suggested by Rommelse and den Nijs.[11]

Interphase	plane	direction	T/K	t/ns	n	L_x/nm	L_y/nm	L_z/nm
i/v	(pI)	[Basal]	248.6	624	8328	36.1163	2.2062	19.0000
i/v	(pI)	[Basal]	242.7	517	6909	36.1013	2.2052	19.0000
i/v	(pI)	[pII]	248.9	483	5700	36.7309	1.8034	19.0000
i/v	(pI)	[pII]	242.4	429	5600	36.7190	1.8028	19.0000
i/w	(pI)	[Basal]	242.2	563	7500	18.0009	2.1991	8.2517
w/v	-	-	242.1	431	5400	18.0059	2.2063	12.0000
i/w	(pI)	[pII]	242.3	529	7060	18.3087	1.7978	8.3431
i/v	(Basal)	[pII]	248.8	1268	10870	18.7696	1.8039	9.3319
i/w	(Basal)	[pII]	248.1	715	9533	18.7696	1.8039	9.3319
i/v	(pII)	[Basal]	248.3	257	3426	18.0577	2.2045	9.5000
i/w	(pII)	[Basal]	248.7	603	8036	18.0134	2.1991	8.0808

TABLE I. Table with detailed description of the simulations performed in this work. For each system studied we describe the interface arrangement, temperature, T , length of simulations, t and size of simulation box L_x , L_y , L_z . All simulations are performed at coexistence.

D. Results for the basal and secondary prismatic planes

We have also studied the fluctuations on the (Basal) and (pII) planes for $\Delta T = -2$ K and the small system sizes (see Table.I). The results seem consistent with the properties of ice microcrystallites (see Fig.2).

The (Basal) plane exhibits a divergence of $\Gamma(q)$ consistent with a smooth interface. A best fit to the model of Eq.4 provides $w = 6.5$ and $g'' = 6.0 \cdot 10^{15}$ J/m⁴, while a constrained fit with $w = 0$ yields $g'' = 12 \cdot 10^{15}$ J/m⁴ and squared deviations that are one order of magnitude larger.

For the (pII) plane we studied the spectrum along (pII)[Basal] and results are suggestive of a rough interface, with $\Gamma(q)$ apparently converging to Σ . Unconstrained fits to the model of Eq.4 yield unphysical results, with a negative w . A constrained fit with $w = 0$ provides $g'' = 3.6 \cdot 10^{15}$ J/m⁴.

As for the (pI) plane, the fluctuations of ice/film and film/vapor surfaces are very well described by results from independent ice/water and water/vapor interfaces. We checked

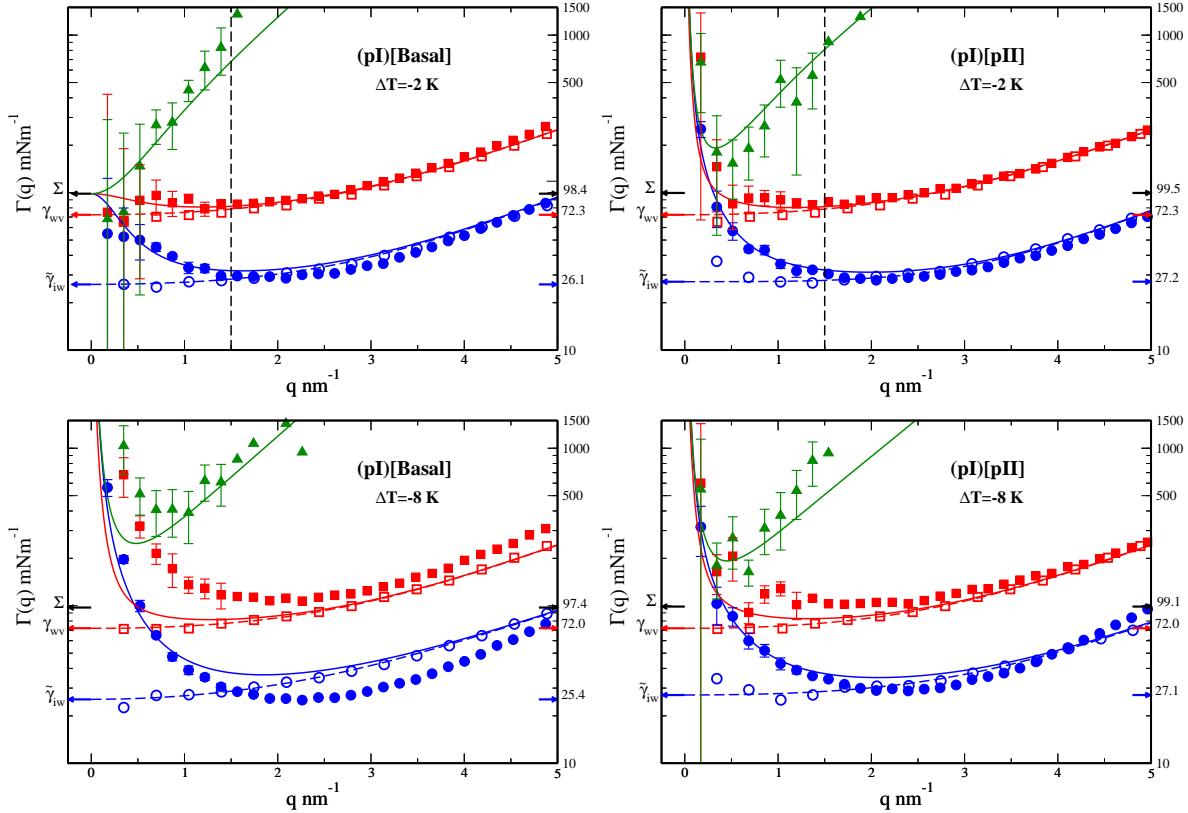


FIG. 1. Fluctuations of the premelting film for the primary prismatic plane at $\Delta T = -2$ K (top) and $\Delta T = -8$ K (bottom). The plot displays wave-vector dependent stiffness, $\Gamma(q)$ in log scale. Left column corresponds to (pI)[Basal], right column to (pI)[pII].

that also the local interfacial structure of the premelting film as described by the density profiles is similar to the independent interfaces, as is seen in Fig.3.

E. Fitting procedure

Fitting of $\Gamma(q)$ to the model of Eq.4 is difficult, because Γ_{iv} is typically orders of magnitude larger than $\Gamma_{if}(q)$ and $\Gamma_{fv}(q)$. For this reason we find it more convenient to fit the results to $1/\Gamma(q)$. In this representation all the results are of similar order of magnitude. Fits were performed by simultaneously adjusting results for $\Gamma_{if}(q)^{-1}$, $\Gamma_{fv}(q)^{-1}$ and $\Gamma_{iv}(q)^{-1}$ with equal weights, from the lowest wave-vector up to $q \approx 4.5$ nm⁻¹. For rough interfaces the $\Gamma(q)^{-1}$ attain a constant value, and for smooth interfaces they vanish as $q \rightarrow 0$.

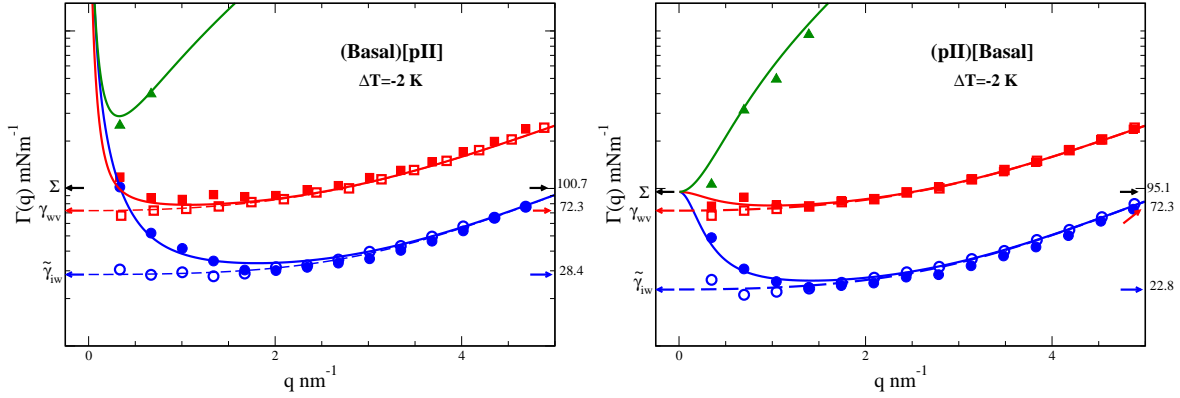


FIG. 2. Fluctuations of the premelting film for basal and secondary prismatic plane. The plot displays $\Gamma(q)$ in log scale for (Basal)[pII] (left) and (pII)[Basal] arrangements, respectively, for temperature $\Delta T = -2$ K. All symbols as in Fig.2 of the paper.

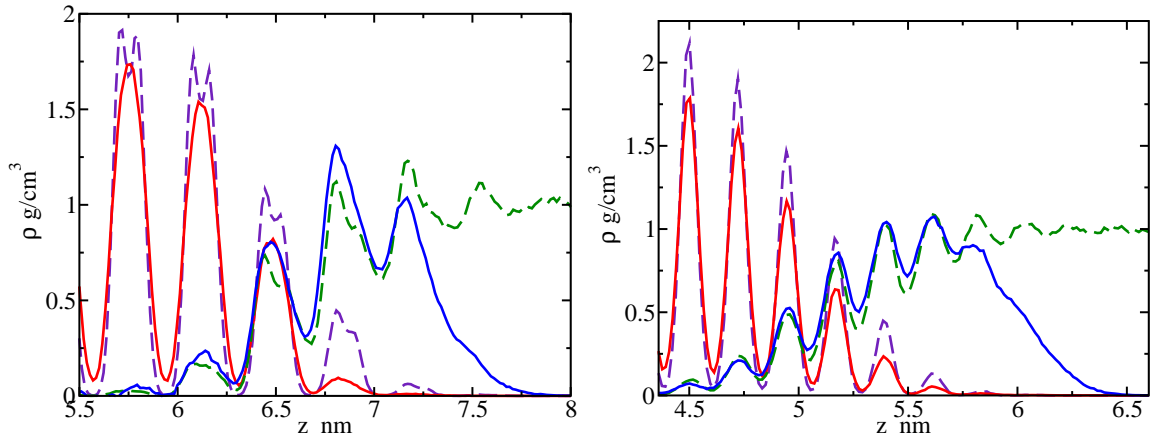


FIG. 3. Density profiles of solid like (dashed line) and liquid like (full line) ice/vapor (full lines) and ice/liquid (dashed lines) interfaces as a function of perpendicular distance z at $\Delta T = -2$ K. From left to right results are shown for the (Basal) and (pII) planes. Rest of captions as in Fig.3 of paper.

F. System size effects

Since the decision as to whether a surface remains rough or smooth requires to study the $q \rightarrow 0$ limit, it is important to assess whether the simulations are subject to system size effects. In Fig.4, we compare $\Gamma(q)$ as obtained for the ice/vapor interface for two different system sizes. The first system size is that reported in the paper, with a long side L_x of about 36 nm. The second is one with equal dimensions for L_y and L_z , but the long

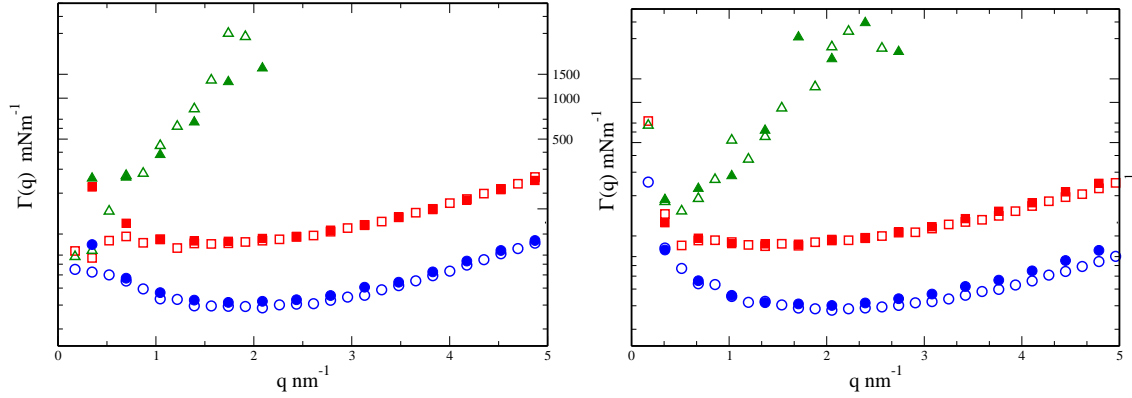


FIG. 4. System size dependence of $\Gamma(q)$ of the ice/vapor interface for the (pI)[Basal] (left) and (pI)[pII] (right) systems studied in this work. Results for the large system with $L_x \approx 36$ nm are shown with empty symbols, and those for the small system with $L_x = 18$ nm are shown with filled symbols.

side L_x half as large. For the (pI)[pII] system, the figure shows no significant system size dependence (though the large system allows for twice as large density of wave-vectors). For the (pI)[Basal] system, again the agreement between large and small systems is very good, up to the lowest wave-vector. In this case we find the largest system exhibits rough behavior, while the small one suggests a smooth interface. We believe this discrepancy is not a system size effect, but rather, a consequence of the neighborhood of the roughening transition and the difficulty to control the temperature within an interval of about 0.5 K.

II. SOLUTION OF THE COUPLED CAPILLARY-WAVE + SINE-GORDON MODEL

A. Model and variational solution

Consider a thin film sandwiched between a solid and a vapor phase. The state of the film is described in terms of a solid/film profile, $h_{\text{if}}(\mathbf{x})$, and a film/vapor profile, $h_{\text{fv}}(\mathbf{x})$, which we denote for short as $h_1(\mathbf{x})$ and $h_2(\mathbf{x})$, respectively. The solid/film interface is described with the sine-Gordon model,[12] and the film/vapor interface with the Capillary Wave Hamiltonian in quadratic approximation.[13] Our coupled Hamiltonian for the quasi-

liquid film is:

$$H_f = \int d\mathbf{x} \left\{ \frac{1}{2} \tilde{\gamma}_{iw} (\nabla h_1)^2 - u \cos(k_z h_1) + \frac{1}{2} \gamma_{wv} (\nabla h_2)^2 + \frac{1}{2} g'' (h_2 - h_1)^2 \right\} \quad (1)$$

where $\tilde{\gamma}_{iw}$ is the stiffness of the ice/water interface, u is a phenomenological coefficient dictating the pinning of the ice/film surface to discrete lattice spacings, $k_z = 2\pi/b$, with b the inter-plane spacing in the direction perpendicular to the interface. γ_{wv} is the liquid/vapor surface tension, and g'' is the second derivative of the interface potential with respect to film thickness. Here it serves as a spring constant for the harmonic fluctuations of the film thickness.[14]

We seek solution of the partition function in terms of the Fourier modes of both surfaces $h_\alpha(\mathbf{q})$ ($\alpha=1$ or 2). Recognizing that the second order approximation of the above result is quadratic in the surface modes, we consider a reference Hamiltonian of independent harmonic oscillators with Gaussian statistics:

$$H_0 = \frac{1}{2} \sum_{\mathbf{q}} \mathbf{h}(\mathbf{q}) \mathbf{G}^{-1}(\mathbf{q}) \mathbf{h}(\mathbf{q}) \quad (2)$$

where $\mathbf{h}(\mathbf{q}) = (h_1(\mathbf{q}), h_2(\mathbf{q}))$ and \mathbf{G}^{-1} is the covariance matrix:

$$\mathbf{G}^{-1}(\mathbf{q}) = \begin{pmatrix} \sigma_{11}^2(\mathbf{q}) & \sigma_{12}^2(\mathbf{q}) \\ \sigma_{21}^2(\mathbf{q}) & \sigma_{22}^2(\mathbf{q}) \end{pmatrix} \quad (3)$$

with matrix components: $\sigma_{11}^2(\mathbf{q}) = \langle h_1(\mathbf{q}) h_1^*(\mathbf{q}) \rangle$, $\sigma_{22}^2(\mathbf{q}) = \langle h_2(\mathbf{q}) h_2^*(\mathbf{q}) \rangle$, $\sigma_{12}^2(\mathbf{q}) = \langle h_1(\mathbf{q}) h_2^*(\mathbf{q}) \rangle$ and $\sigma_{21}^2(\mathbf{q}) = \langle h_2(\mathbf{q}) h_1^*(\mathbf{q}) \rangle$.

The partition function of the reference Hamiltonian is:[15]

$$Z_0 = \int \prod_{\mathbf{q}} d\mathbf{h}(\mathbf{q}) e^{-\frac{1}{2} \beta \sum_{\mathbf{q}} \mathbf{h}(\mathbf{q}) \mathbf{G}^{-1}(\mathbf{q}) \mathbf{h}(\mathbf{q})} \quad (4)$$

while the free energy is:

$$F_0 = \frac{1}{2} k_B T \sum_{\mathbf{q}} \ln \frac{\det \mathbf{G}^{-1}(\mathbf{q})}{(2\pi k_B T)^2} \quad (5)$$

This result can be expressed explicitly in terms of the elements of the covariance matrix:

$$F_0 = -\frac{1}{2} k_B T \sum_{\mathbf{q}} \ln [(2\pi k_B T)^2 (\sigma_{11}^2(\mathbf{q}) \sigma_{22}^2(\mathbf{q}) - \sigma_{12}^4(\mathbf{q}))] \quad (6)$$

Next, we assess the free energy contribution from H_f by performing an average over the Gaussian statistics of the reference oscillators, $F_f = \langle H_f \rangle_0$, with the result:

$$F_f = \frac{1}{2} A \sum_{\mathbf{q}} \left\{ [g'' + \tilde{\gamma}_{iw} q^2] \sigma_{11}^2(q) + [g'' + \gamma_{wv} q^2] \sigma_{22}^2(q) - 2g'' \sigma_{12}^2(q) - u e^{-\frac{1}{2} k_z^2 \sum_{\mathbf{q}} \sigma_{11}^2(q)} \right\} \quad (7)$$

where q is the norm of \mathbf{q} . Notice we have taken into account that the Gaussian average of $\cos(k_z h_1(\mathbf{x}))$ is $\exp(-\frac{1}{2}k_z^2 \langle h_1^2(\mathbf{x}) \rangle)$, and further used Parseval's theorem to transform averages of $h_1^2(\mathbf{x})$ and $h_2^2(\mathbf{x})$ into averages of their Fourier components.

The total free energy is $F_0 + F_f$, and we obtain a solution in closed form by seeking for the variational parameters $\sigma_{11}^2(q)$, $\sigma_{22}^2(q)$ and $\sigma_{12}^2(q)$. The result of this minimization yields:

$$\begin{aligned}\sigma_{11}^2(q) &= \frac{k_B T}{A} \frac{g'' + \gamma_{wv} q^2}{[w + g'' + \tilde{\gamma}_{iw} q^2][g'' + \gamma_{wv} q^2] - g''^2} \\ \sigma_{22}^2(q) &= \frac{k_B T}{A} \frac{w + g'' + \tilde{\gamma}_{iw} q^2}{[w + g'' + \tilde{\gamma}_{iw} q^2][g'' + \gamma_{wv} q^2] - g''^2} \\ \sigma_{12}^2(q) &= \frac{k_B T}{A} \frac{g''}{[w + g'' + \tilde{\gamma}_{iw} q^2][g'' + \gamma_{wv} q^2] - g''^2}\end{aligned}\tag{8}$$

where the roughness parameter w is

$$w = uk_z^2 e^{-\frac{1}{2}k_z \Sigma_q} \sigma_{11}^2(q)\tag{9}$$

To solve for this self consistent condition, we ignore surface anisotropy, which is small for ice (see next section), and approximate:

$$\sum_{\mathbf{q}} \sigma_{11}^2(q) = \frac{k_B T}{2\pi} \int_0^{q_{max}} q dq \frac{g'' + \gamma_{wv} q^2}{wg'' + (g''\Sigma + w\gamma_{wv})q^2 + \gamma^2 q^4}\tag{10}$$

where q_{max} is an ultra-violet cut-off and we have introduced $\Sigma = \tilde{\gamma}_{iw} + \gamma_{wv}$ and $\gamma^2 = \tilde{\gamma}_{iw}\gamma_{wv}$ for short.

This integral may be solved in real space along the lines indicated in Ref.[16], with the result:

$$\sum_{\mathbf{q}} \sigma_{11}^2(q) = C \ln\left(1 + \frac{pr}{wg''} q_{max}^2\right) + D \ln\left(1 + \frac{\gamma^2}{pr} q_{max}^2\right)\tag{11}$$

where:

$$p = g''\Sigma + w\gamma_{wv}\tag{12}$$

$$r = \frac{p + (p^2 - 4wg''\gamma^2)^{1/2}}{2p}\tag{13}$$

$$C = \frac{k_B T}{4\pi} \frac{g''rp - g''\gamma_{wv}w}{r^2p^2 - wg''\gamma^2}\tag{14}$$

$$D = \frac{k_B T}{4\pi} \frac{pr \gamma_{wv}rp - g''\gamma^2}{\gamma^2 r^2p^2 - wg''\gamma^2}\tag{15}$$

For H₂O, where $\gamma_{wv} > \tilde{\gamma}_{iw}$ at the triple point, r is always positive and real.

As we shall see, the outcome of the self consistent condition is mainly dictated by the behavior of Eq. (11) at small w , whence, we assume $p^2 \gg 4wg''\gamma^2$, so that expanding the square root in Eq. (13) to zero order, the coefficients C and D simplify to:

$$C = \frac{k_B T}{4\pi} \frac{g''^2 \Sigma}{(g'' \Sigma + w\gamma_{wv})^2} \quad (16)$$

and

$$D = \frac{k_B T}{4\pi} \frac{\gamma_{wv}}{\tilde{\gamma}_{iw}} \frac{g'' + w}{g'' \Sigma + w\gamma_{wv}} \quad (17)$$

By use of Eq. (9), Eq. (11) and Eq.16-17, we obtain the self-consistent condition in closed form as:

$$w = uk_z^2 \left(1 + \frac{g'' \Sigma + w\gamma_{wv}}{wg''} q_{max}^2 \right)^{-\mu} \cdot \left(1 + \frac{\gamma^2}{g'' \Sigma + w\gamma_{wv}} q_{max}^2 \right)^{-\tau} \quad (18)$$

where $\mu = \frac{1}{2}k_z^2 C$ and $\tau = \frac{1}{2}k_z^2 D$.

In order to understand the significance of this result, let us first consider the case of the ice/water interface (film of infinite thickness), such that $g'' \equiv 0$. In that case, $\mu \equiv 0$, and we get:

$$w = uk_z^2 \left(1 + \frac{\tilde{\gamma}_{iw}}{w} q_{max}^2 \right)^{-\tau_{iw}} \quad (19)$$

with $\tau_{iw} = \frac{\pi k_B T}{2\tilde{\gamma}_{iw} b^2}$. It follows that w is the real root of the auxiliary equation $x = y(x)$, with

$$y(x) = \left(1 + \frac{a}{x} \right)^{-\tau_{iw}} \quad (20)$$

and a a constant. i.e., w is given by the intersection of a straight line of unit slope with the auxiliary function $y(x)$. This function goes through the origin with positive slope, then bends and eventually becomes constant. For $\tau_{iw} < 1$, $y(x)$ meets the origin with infinite slope, and must therefore cross the straight line of unit slope at finite x . If, on the other hand, $\tau_{iw} > 1$, $y(x)$ meets the origin with zero slope and there is only one root at $x = 0$ (see Fig.5). Whence, we encounter a roughening transition from a smooth surface (finite w) to a rough surface ($w = 0$) at $\tau_{iw} = 1$. [17] This corresponds exactly to the roughening transition of the sine-Gordon model. [12]

Let us now consider the general case of an ice surface covered by a quasi-liquid film of finite depth, with finite g'' . The solutions for w are now given by Eq. (18), which, in the limit $w \ll g''$ becomes:

$$w = uk_z^2 \left(1 + \frac{\Sigma}{w} q_{max}^2 \right)^{-\mu_{if}} \cdot \left(1 + \frac{\gamma^2}{g'' \Sigma} q_{max}^2 \right)^{-\tau_{if}} \quad (21)$$

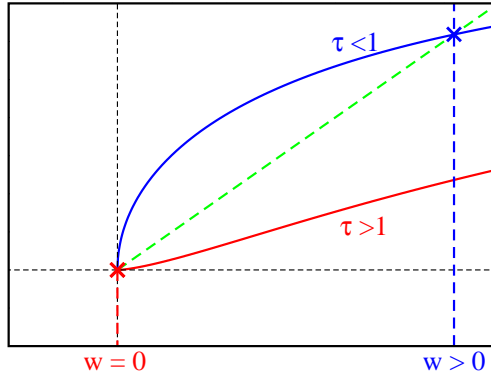


FIG. 5. Sketch of the solution of $w \propto y(w)$ dictating the roughness of a solid/liquid interface. The green line is a straight line of unit slope. Blue and red lines correspond to $y(w)$ (Eq. (20)) for $\tau > 1$ and $\tau < 1$, respectively. The equilibrium roughness w is given by the intersection of either curve with the straight green line. For $\tau > 1$, only one root at $w = 0$ exists (rough interface). For $\tau < 1$, an additional route $w > 0$ is found (smooth interface).

where $\mu_{if} = \frac{\tilde{\gamma}_{iw}}{\Sigma} \cdot \tau_{iw}$ and $\tau_{if} = \frac{\gamma_{wv}}{\Sigma} \cdot \tau_{iw}$. This result shows the dramatic consequences of pinning the liquid film on the ice surface. Particularly, the second parenthesis of the right hand side, which drives the roughening transition for the case $g'' \equiv 0$, is now a constant. On the other hand, the first parenthesis, which was unity in that case, becomes responsible for driving the roughening transition. In fact, it takes exactly the same form as Eq. (19), albeit, with a completely different exponent, which differs from τ_{iw} by a factor $\tilde{\gamma}_{iw}/\Sigma$. For our model, this is about 1/3 at the triple point. The implication is that under conditions where the ice/water surface has become rough, with $\tau_{iw} \geq 1$, we expect that μ_{if} will be largely below unity. Hence, the coupling of the film/vapor interface to the ice/film surface via g'' drives the rough ice/water interface into a smooth surface. In practice, the effect is significant for large g'' . For finite but small g'' , the root occurs extremely close to $w = 0$, and the smoothing is then only apparent at very large length-scales. Our results are consistent with previous studies showing the sensitivity of roughening to monolayer surface adsorption.[18]

B. Roughening anisotropy

Ordinary ice has hexagonal symmetry and is therefore not strictly isotropic. Particularly, for the ice/water interface at $\Delta T = -2$ K, the (pI) crystal plane has slightly different principal stiffness coefficients for the [Basal] (call it x) and [pII] (call it y) directions (i.e., $\tilde{\gamma}_{iw}(x) = 26.14$ mN/m and $\tilde{\gamma}_{iw}(y) = 27.18$ mn/m, respectively). To account for this anisotropy, the Hamiltonian of Eq. (1) should be replaced by:

$$H_f = \int d\mathbf{x} \left\{ \frac{1}{2} \tilde{\gamma}_{iw}(x) \left(\frac{\partial h_1}{\partial x} \right)^2 + \frac{1}{2} \tilde{\gamma}_{iw}(y) \left(\frac{\partial h_1}{\partial y} \right)^2 - u \cos(k_z h_1) + \frac{1}{2} \gamma_{wv} (\nabla h_2)^2 + \frac{1}{2} g'' (h_2 - h_1)^2 \right\} \quad (22)$$

The solution of this Hamiltonian in Fourier modes is exactly as for the isotropic case, provided one replaces $\tilde{\gamma}_{iw} q^2$ by $\tilde{\gamma}_{iw}(x) q_x^2 + \tilde{\gamma}_{iw}(y) q_y^2$. [19] Particularly, the result for σ_{11}^2 in Eq. (8) should be replaced by:

$$\sigma_{11}^2(\mathbf{q}) = \frac{k_B T}{A} \frac{g'' + \gamma_{wv} q^2}{[w + g'' + \tilde{\gamma}_{iw}(x) q_x^2 + \tilde{\gamma}_{iw}(y) q_y^2][g'' + \gamma_{wv} q^2] - g''^2} \quad (23)$$

For large but finite surfaces of circular or square shape the sum $\sum_{\mathbf{q}} \sigma_{11}^2(\mathbf{q})$ required to measure w in Eq. (9) is effectively performed from a low wave-vector $\mathbf{q} = (\frac{2\pi}{L}, \frac{2\pi}{L}) \rightarrow (0, 0)$, and the anisotropy of the stiffness coefficients is inconsequential. [20]

In our systems, however, we study surfaces that are very thin in one direction and large in the other. Accordingly, the large wave-length modes in the short direction are cut-off and the lower cut-off is anisotropic, since now $\mathbf{q} = (\frac{2\pi}{L_x}, \frac{2\pi}{L_y})$ and $L_x \neq L_y$. Whence, for the (pI)[Basal] direction we have an effective lower cut-off at $\mathbf{q} = (0, \frac{2\pi}{L_y})$, while in the (pI)[pII] direction the lower-cut-off is $\mathbf{q} = (\frac{2\pi}{L_x}, 0)$. As a result, the sum $\sum_{\mathbf{q}} \sigma_{11}^2(\mathbf{q})$ now depends on the system geometry. Accordingly, the self-consistent condition for the roughness parameter, Eq. (9), also becomes anisotropic.

The effect is weak, however, because the anisotropy in the stiffness coefficient is small. Indeed, for the crystal/melt interface of NaCl we have checked previously that for systems well above the roughening transition, the results for an elongated system are fully equivalent to those of a square interface. [21]

In our case the problem is more subtle, because we are close to the roughening transition. Unfortunately, this effect cannot be described analytically, because the integral of Eq. (23) can be solved in circular coordinates, but not in rectangular coordinates as required here. [20]

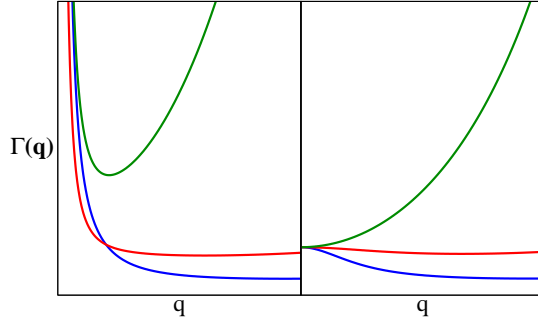


FIG. 6. Results for $\Gamma(q)$ as obtained from the model of Eq. (8) for the ice/film (blue), film/vapor (red) and coupled fluctuations of the ice/film and film/vapor surfaces (green). Left: Behavior expected for a smooth interface, with finite g'' and w . Right: Behavior expected for a rough interface, with finite g'' but $w = 0$.

Nevertheless, assuming we can obtain the root of w using the exponent μ_{if} for the isotropic case by merely replacing $\Sigma = \gamma_{lv} + \tilde{\gamma}_{iw}$ with the corresponding anisotropic stiffness, we find the exponent for roughening in the (pI)[Basal] direction is $\approx (72 + 27)/(72 + 26) = 1.01$ times larger than that for the (pI)[pII] direction, whence, the (pI)[Basal] system may become effectively rough at a temperature where (pI)[pII] remains smooth, as observed in our simulations.

C. Asymptotic behavior of the surface fluctuations

The behavior of the surface Fourier modes adopts distinct behavior in the limit $q \rightarrow 0$, depending on whether g'' and w are null or finite (Fig.6).

This allows to tell whether the surface is rough ($w = 0$) or smooth $w > 0$ from the behavior of the spectrum of fluctuations.

Defining:

$$\begin{aligned}
 \Gamma_{if}(q) &= \frac{k_B T}{A \langle h_{if}(q) h_{if}^*(q) \rangle q^2} \\
 \Gamma_{fv}(q) &= \frac{k_B T}{A \langle h_{fv}(q) h_{fv}^*(q) \rangle q^2} \\
 \Gamma_{iv}(q) &= \frac{k_B T}{A \langle h_{if}(q) h_{fv}^*(q) \rangle q^2}
 \end{aligned} \tag{24}$$

we find, from Eq. (8):

: Limit of $q \rightarrow \infty$.

For sufficiently large q , both surfaces of the quasi-liquid layer behave like rough and independent ice/water and water/vapor interfaces:

$$\begin{aligned}\Gamma_{\text{if}}(q) &\rightarrow \tilde{\gamma}_{iw} \\ \Gamma_{\text{fv}}(q) &\rightarrow \gamma_{wv} \\ \Gamma_{\text{iv}}(q) &\rightarrow \frac{q^2}{g''}\end{aligned}\tag{25}$$

: Limit of $q \rightarrow 0$.

In the limit of small q , the behavior is distinctly different depending on whether the ice/vapor interface is smooth ($w > 0$) or rough ($w = 0$):

: Smooth interface ($w > 0$).

For a smooth interface, the fluctuations remain finite at zero wave-vector, and the $\Gamma_{\alpha\beta}$ diverge.

$$\begin{aligned}\Gamma_{\text{if}}(q) &\rightarrow \frac{w}{q^2} \\ \Gamma_{\text{fv}}(q) &\rightarrow \frac{wg''}{(g''+w)q^2} \\ \Gamma_{\text{iv}}(q) &\rightarrow \frac{w}{q^2}\end{aligned}\tag{26}$$

: Rough interface ($w = 0$).

For a rough interface, the fluctuations diverge and the interface behaves globally as a rough surface with stiffness $\Sigma = \tilde{\gamma}_{iw} + \gamma_{wv}$.

$$\begin{aligned}\Gamma_{\text{if}}(q) &\rightarrow \Sigma \\ \Gamma_{\text{fv}}(q) &\rightarrow \Sigma \\ \Gamma_{\text{iv}}(q) &\rightarrow \Sigma\end{aligned}\tag{27}$$

Notice that the latter behavior is also observed for a smooth interface in the range of wave-vectors $g''w \ll g''\Sigma q^2 \ll \gamma^2 q^4$ provided $w \ll g''$. Therefore, for very small w it is required to attain a regime of very small q to discriminate between a rough and a smooth surface.

[1] J. L. F. Abascal and C. Vega, J. Chem. Phys. **123**, 234505 (2005).

[2] V. Buch, P. Sandler, and J. Sadlej, J. Phys. Chem. B **102**, 8641 (1998).

[3] S. W. Rick and A. D. J. Haymet, J. Chem. Phys. **118**, 9291 (2003).

- [4] L. G. MacDowell and C. Vega, *J. Phys. Chem. B* **114**, 6089 (2010).
- [5] D. Rozmanov and P. G. Kusalik, *Phys. Chem. Chem. Phys.* **13**, 15501 (2011).
- [6] G. Bussi, D. Donadio, and M. Parrinello, *J. Chem. Phys.* **126**, 014101 (2007).
- [7] R. L. Davidchack, J. R. Morris, and B. B. Laird, *J. Chem. Phys.* **125**, 094710 (2006).
- [8] J. Benet, L. G. MacDowell, and E. Sanz, *J. Chem. Phys.* **141**, 034701 (2014).
- [9] J. Benet, L. G. MacDowell, and E. Sanz, *Phys. Chem. Chem. Phys.* **16**, 22159 (2014).
- [10] W. Lechner and C. Dellago, *J. Chem. Phys.* **129**, 114707 (2008).
- [11] K. Rommelse and M. den Nijs, *Phys. Rev. Lett.* **59**, 2578 (1987).
- [12] P. M. Chaikin and T. C. Lubensky, *Principles of Condensed Matter Physics* (Cambridge University Press, Cambridge, 1995).
- [13] D. Nelson, T. Piran, and S. Weinberg, *Statistical Mechanics of Membranes and Surfaces* (Word Scientific, Singapore, 2004).
- [14] S. Dietrich, in *Phase Transitions and Critical Phenomena*, Vol. 12, edited by C. Domb and J. L. Lebowitz (Academic, New York, 1988) pp. 1–89.
- [15] N. Goldenfeld, *Lectures on Phase Transitions and the Renormalization Group* (Perseus Books, Reading, Massachusetts, 1992).
- [16] L. G. MacDowell, [cond-mat.soft], ArXiv:1512.04777 (2015).
- [17] S. A. Safran, *Statistical Thermodynamics of Surfaces, Interfaces and Membranes*, 1st ed. (Addison-Wesley, Reading, 1994).
- [18] N. Akutsu, Y. Akutsu, and T. Yamamoto, *Phys. Rev. B* **64**, 085415 (2001).
- [19] D. S. Fisher and J. D. Weeks, *Phys. Rev. Lett.* **50**, 1077 (1983).
- [20] N. Akutsu and T. Yamamoto, in *Handbook of Crystal Growth (Second Edition)*, edited by T. Nishinaga (Elsevier, Boston, 2015) second edition ed., pp. 265–313.
- [21] J. Benet, L. G. MacDowell, and E. Sanz, *J. Chem. Phys.* **142**, 134706 (2015), <http://dx.doi.org/10.1063/1.4916398>.